Terahertz imaging employing graphene modulator arrays

Berardi Sensale-Rodriguez,[*] Subrina Rafique, Rusen Yan, Mingda Zhu, Vladimir Protasenko, Debdeep Jena, Lei Liu, and Huili Grace Xing[1]

Department of Electrical Engineering, University of Notre Dame, Notre Dame, IN 46556, USA
[1] hxing@nd.edu
**bsensale@nd.edu*

Abstract: In this paper we propose and experimentally demonstrate arrays of graphene electro-absorption modulators as electrically reconfigurable patterns for terahertz cameras. The active element of these modulators consists of only single-atom-thick graphene, achieving a modulation of the THz wave reflectance > 50% with a potential modulation depth approaching 100%. Although the prototype presented here only contains 4x4 pixels, it reveals the possibility of developing reliable low-cost video-rate THz imaging systems employing single detector.

OCIS codes: (110.6795) Terahertz imaging; (230.4110) Modulators; (160.4236) Nanomaterials.

References and links

1. M. Tonouchi, "Cutting-edge terahertz technology," Nat. Photonics **1**(2), 97–105 (2007).
2. W. L. Chan, J. Deibel, and D. Mittleman, "Imaging with terahertz radiation," Rep. Prog. Phys. **70**(8), 1325–1379 (2007).
3. J. F. Federici, B. Schulkin, F. Huang, D. Gary, R. Barat, F. Oliveira, and D. Zimdars, "THz imaging and sensing for security applications—explosives, weapons and drugs," Semicond. Sci. Technol. **20**(7), S266–S280 (2005).
4. H.-B. Liu, H. Zhong, N. Karpowicz, Y. Chen, and X.-C. Zhang, "Terahertz Spectroscopy and Imaging for Defense and Security Applications," Proc. IEEE **95**(8), 1514–1527 (2007).
5. J. B. Jackson, M. Mourou, J. F. Whitaker, I. N. Duling III, S. L. Williamson, M. Menu, and G. A. Mourou, "Terahertz imaging for non-destructive evaluation of mural paintings," Opt. Commun. **281**(4), 527–532 (2008).
6. J. L. Tomaino, A. D. Jameson, J. W. Kevek, M. J. Paul, A. M. van der Zande, R. A. Barton, P. L. McEuen, E. D. Minot, and Y.-S. Lee, "Terahertz imaging and spectroscopy of large-area single-layer graphene," Opt. Express **19**(1), 141–146 (2011).
7. J. D. Buron, D. H. Petersen, P. Bøggild, D. G. Cooke, M. Hilke, J. Sun, E. Whiteway, P. F. Nielsen, O. Hansen, A. Yurgens, and P. U. Jepsen, "Graphene conductance uniformity mapping," Nano Lett. **12**(10), 5074–5081 (2012).
8. A. J. Fitzgerald, E. Berry, N. N. Zinovev, G. C. Walker, M. A. Smith, and J. M. Chamberlain, "An introduction to medical imaging with coherent terahertz frequency radiation," Phys. Med. Biol. **47**(7), R67–R84 (2002).
9. S. Nakajima, H. Hoshina, M. Yamashita, C. Otani, and N. Miyoshi, "Terahertz imaging diagnostics of cancer tissues with a chemometrics technique," Appl. Phys. Lett. **90**(4), 041102 (2007).
10. Z. Jiang and X.-C. Zhang, "Terahertz imaging via electrooptic effect," IEEE Trans. Microw. Theory Tech. **47**(12), 2644–2650 (1999).
11. B. B. Hu and M. C. Nuss, "Imaging with terahertz waves," Opt. Lett. **20**(16), 1716–1718 (1995).
12. D. Zimdars, "High speed terahertz reflection imaging," Proc. SPIE **5692**, 255–259 (2005).
13. J. Xu and X.-C. Zhang, "Terahertz wave reciprocal imaging," Appl. Phys. Lett. **88**(15), 151107 (2006).
14. W. L. Chan, K. Charan, D. Takhar, K. F. Kelly, R. G. Baraniuk, and D. M. Mittleman, "A single-pixel terahertz imaging system based on compressed sensing," Appl. Phys. Lett. **93**(12), 121105 (2008).
15. W. L. Chan, H.-T. Chen, A. J. Taylor, I. Brener, M. J. Cich, and D. M. Mittleman, "A spatial light modulator for terahertz beams," Appl. Phys. Lett. **94**(21), 213511 (2009).
16. B. Sensale-Rodriguez, T. Fang, R. Yan, M. M. Kelly, D. Jena, L. Liu, and H. G. Xing, "Unique prospects for graphene-based terahertz modulators," Appl. Phys. Lett. **99**, 113104 (2011).
17. B. Sensale-Rodriguez, R. Yan, M. M. Kelly, T. Fang, K. Tahy, W. S. Hwang, D. Jena, L. Liu, and H. G. Xing, "Broadband graphene terahertz modulators enabled by intraband transitions," Nat Commun **3**, 780 (2012).
18. B. Sensale-Rodriguez, R. Yan, S. Rafique, M. Zhu, W. Li, X. Liang, D. Gundlach, V. Protasenko, M. M. Kelly, D. Jena, L. Liu, and H. G. Xing, "Extraordinary control of terahertz beam reflectance in graphene electro-absorption modulators," Nano Lett. **12**(9), 4518–4522 (2012).
19. S. H. Lee, M. Choi, T.-T. Kim, S. Lee, M. Liu, X. Yin, H. K. Choi, S. S. Lee, C.-G. Choi, S.-Y. Choi, X. Zhang, and B. Min, "Switching terahertz waves with gate-controlled active graphene metamaterials," Nat. Mater. **11**(11), 936–941 (2012).

#180110 - $15.00 USD Received 19 Nov 2012; revised 13 Jan 2013; accepted 14 Jan 2013; published 23 Jan 2013

20. X. Li, W. Cai, J. An, S. Kim, J. Nah, D. Yang, R. Piner, A. Velamakanni, I. Jung, E. Tutuc, S. K. Banerjee, L. Colombo, and R. S. Ruoff, "Large-area synthesis of high-quality and uniform graphene films on copper foils," Science **324**(5932), 1312–1314 (2009).
21. L. Liu, J. L. Hesler, R. M. Weikle, T. Wang, P. Fay, and H. G. Xing, "A 570-630 GHz frequency domain spectroscopy system based on a broadband quasi-optical Schottky diode detector," Int. J. High Speed Electron. Syst. **20**, 629–638 (2011).
22. L. Liu, J. L. Hesler, H. Xu, A. W. Lichtenberger, and R. M. Weikle, "A broadband quasi-optical terahertz detector using a zero bias Schottky diode," IEEE Microw. Wireless Compon. Lett. **20**(9), 504–506 (2010).
23. D. B. M. Klaassen, "A unified mobility model for device simulation – I. Model equations and concentration dependence," Solid-State Electron. **35**(7), 953–959 (1992).
24. N. M. R. Peres and T. Stauber, "Transport in a clean graphene sheet at finite temperature and frequency," Int. J. Mod. Phys. B **22**(16), 2529–2536 (2008).
25. R. Yan, B. Sensale-Rodriguez, L. Liu, D. Jena, and H. G. Xing, "A new class of electrically tunable metamaterial terahertz modulators," Opt. Express **20**(27), 28664–28671 (2012).
26. B. Sensale-Rodriguez, R. Yan, M. Zhu, D. Jena, L. Liu, and H. G. Xing, "Efficient terahertz electro-absorption modulation employing graphene plasmonic structures," Appl. Phys. Lett. **101**(26), 261115 (2012).
27. L. Ju, B. Geng, J. Horng, C. Girit, M. Martin, Z. Hao, H. A. Bechtel, X. Liang, A. Zettl, Y. R. Shen, and F. Wang, "Graphene plasmonics for tunable terahertz metamaterials," Nat. Nanotechnol. **6**(10), 630–634 (2011).

1. Introduction

The terahertz (THz) frequency range, until recently one of the least explored areas of the electromagnetic spectrum, is gaining attention by the scientific research community due to its important applications in diverse disciplines such as astronomy, biological and chemical sensing, communications, security, etc [1]. THz waves are attractive for several imaging applications, since they can propagate through non metallic media such as paper, cloth, plastics, and ceramics, and do not scatter over nano-scale defects or ionize the material under imaging -as might shorter wavelengths do- while offering an image resolution similar to that of the human eye [2]. Some of these applications include defense and security inspection [3, 4], non-destructive testing [5], contact-less material characterization [6, 7], biological imaging [8, 9], and so on. To this end, there is an increasing demand for compact high-performance low-cost THz imagers operating at room temperature.

Several methods have been proposed for THz imaging in the literature [10–15]. In this paper, we focus on active imaging, i.e. a THz source is used to illuminate the object under detection. Systems employing arrays of sources or detectors can achieve real time operation, e.g. focal-plane detector arrays used in RF and IR/Vis systems where high performance and cost-effective components are available. However, in the THz range such systems are highly complex and expensive. Furthermore, the performance of detectors used in a THz focal plane array can be compromised in comparison to a single optimized detector. An additional advantage of a single detector is that it can be easily combined with high quality collection optics. Therefore, single-detector THz scanning imaging systems [13] are particularly attractive since they can benefit from the superior detection sensitivity of an optimized detector as well as the coherence of a single-point source. In a scanning system, one can use a mechanical stage to scan either the object or the detector or an aperture [14, 15] to obtain an image. Though such a system is simple to implement, the image acquisition rates are very low because of the mechanical stages used and sequential acquisition of pixels. On the other hand, one can replace the slow mechanical stage with an electronically reconfigurable modulator array with fast switching speed to achieve real time imaging. Recently, high performance graphene THz electro-absorption modulators [16–19] have been demonstrated, which are also facile and inexpensive to fabricate. In this work, we present our first step toward demonstrating low-cost real-time THz imager using arrays of graphene based electro-absorption modulators.

2. Device structure and THz measurement setup

The modulator array was made of large area CVD grown [20] single layer graphene, which was subsequently transferred into a SiO_2/p-Si substrate employing poly(methyl methacrylate) PMMA and wet etch methods. The *p*-Si is lightly doped with a high resistivity ρ of ~1000 Ω.cm to minimize substrate attenuation. The 70-nm thick SiO_2 was thermally grown. The

#180110 - $15.00 USD Received 19 Nov 2012; revised 13 Jan 2013; accepted 14 Jan 2013; published 23 Jan 2013

large area graphene layer was patterned using O_2 plasma into an array of 4x4 squares with an area of 0.7 x 0.7 mm^2 per square or pixel and a pixel-pixel separation of 100 µm. The top ring metal contacts (Ti/Au) were deposited along the periphery of each graphene square so that each pixel can be independently biased. A continuous metal layer of Ti/Au was deposited on the backside of the substrate to act as both a reflector and electrode, therefore, the THz reflection is modulated. The reflection modulation is chosen over the transmission mode since the reflection modulator exhibits higher modulation depth as a result of the electromagnetic wave field concentration [18]. A schematic structure of the modulator array and an optical image of the device are presented in Figs. 1(a) and 1(b), respectively.

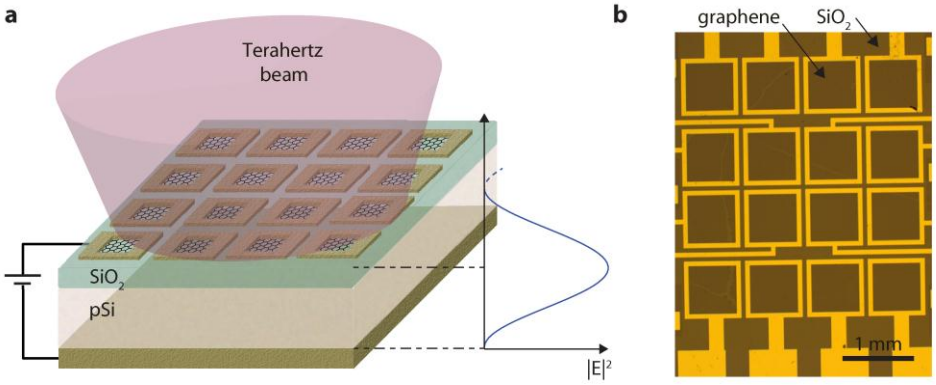

Fig. 1. (a) Schematic and (b) optical image of the graphene reflection modulator array. The pixel size is 0.7x0.7 mm^2. As shown in (a) the electric field intensity at the active graphene enhances by 4 times when the substrate optical thickness is an odd multiple of the quarter wavelength of the incoming THz radiation, thus leading to augmented modulation in reflectance in comparison to the transmission mode [18].

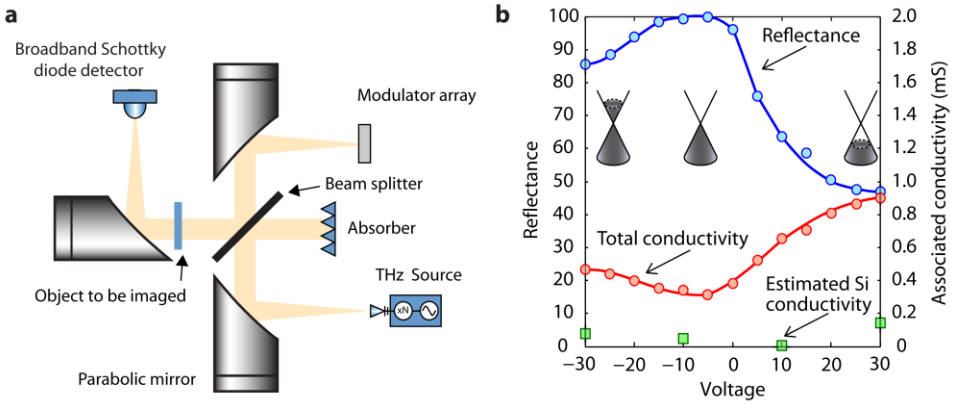

Fig. 2. (a) Sketch of the reflectance mode THz quasi-optical setup. (b) Measured reflectance (blue circles) and associated conductivity (red circles) versus voltage when the same voltage was applied between all the pixels and the back contact. The radiation was focused onto the center of the modulator array and the frequency was set at 590 GHz so that the substrate optical thickness is matched to be an odd quarter of the THz wavelength. The estimated conductivity contribution of carriers in the Si substrate is shown in green squares.

The modulator array was characterized using a terahertz imaging and spectroscopy setup [21] based on a Virginia Diodes, Inc. (VDI) multiplier source, capable of providing continuous wave (CW) radiation in the 570 - 630 GHz frequency band, and a broadband Schottky diode detector [22]. A schematic of the device characterization and imaging setup is shown in Fig. 2(a), and the exact locations of the modulator array and the objects imaged are

#180110 - $15.00 USD Received 19 Nov 2012; revised 13 Jan 2013; accepted 14 Jan 2013; published 23 Jan 2013

described in each measurement detailed in the later sections. All the experiments were carried out at room temperature. The beam was at normal incidence to the modulators and the objects imaged.

3. Principle and verification of modulator operation

The electrical modulation or reconfigurability in these graphene-SiO_2-Si structures has been detailed in our previous work [16–18]. Here we provide a summary of its operation mechanism. When the applied voltage between the top graphene and the back electrode is such that the Fermi level in graphene is at the Dirac point ($V = V_{CNP}$), both DC and THz optical conductivity of graphene is at the minimum, i.e. THz absorption by graphene is minimal. When a voltage is applied so that the Fermi level moves away from the Dirac point, the optical conductivity of graphene increases thus its absorption of the THz wave. Modulation of the free carriers in the Si substrate has an insignificant impact on the device characteristics [17], which is also supported by CV measurements in this work. Using the carrier distribution in the Si substrate as a function of the applied voltage estimated from Shrodinger-Poisson self-consistent simulations, and assuming a concentration dependent mobility [23], we calculated the conductivity of the whole Si substrate from the SiO_2/Si interface to the back contact. Our estimations show that the contribution from graphene alone to the total conductivity of the graphene/SiO_2/Si structure is >80% in the entire measured voltage range, thus the observed THz modulation is mainly owed to the carrier dynamics in the graphene layer. Though the best experimentally demonstrated range of graphene tunable conductivity promises near unity modulation in the transmission mode, the practical tunable range of large area graphene achievable today (~0.15 to ~1mS) limits the modulation depth to ~20% [17]. One way to improve modulation is to place the active graphene layers at the maximum field region in a cavity. To this end, we have demonstrated THz reflectance modulators [18], where the electric field at the graphene layer can be enhanced by 4 times when the optical thickness of the substrate is an odd multiple of a quarter-wavelength of the incoming THz radiation. The field distribution under this condition is depicted in Fig. 1(a). The minimum conductivity of graphene (~0.15 mS [24]) leads to a theoretical insertion loss of ~20% in reflectance based modulators [18].

To demonstrate the graphene array shown in Fig. 1 indeed functions as a reflectance modulator, the reflectance was measured when sweeping the bias between the top contacts (by shorting all pixels) and the back contact. The device was placed at the focal plane in the reflectance optical setup (Fig. 2), and the pixel at Row 2 and Column 2 was approximately situated within the beam waist, which is < 1 mm at its minimum [21]. Shown in Fig. 2(b) are the measured reflectance and the associated total conductivity of the device at a frequency where the substrate optical thickness is matched to be an odd quarter wavelength of the THz radiation. The estimated upper bound of the conductivity of the entire Si substrate is also shown to support the dominant role of graphene in the device operation. The Dirac point in graphene is found to be near V = −10 V, as evidenced by the highest reflectivity; and a clear transition from *n* to *p*-type in graphene is also observed (reflectance monotonically decreases with $| V - V_{CNP} |$). More detailed characterizations, with the THz beam focused on different positions of the modulator array, showed a spatial variation of the Dirac point voltage in the range of −5 to −11 V. The broad reflection minima in Fig. 2(b) is attributed to the doping inhomogeneity across the graphene, however other factors might also contribute to this behavior, further investigations are required to better clarify the origin of this observation. The modulation depth, always defined as $(R_{high}-R_{low})/R_{high}$, was found to vary between ~50 to ~30% across the device, with 2 out of 16 pixels not showing any modulation. Since the minimum beam waist (< ~1 mm diameter) is comparable to the pixel dimension (0.7 x 0.7 mm^2), local information about the graphene quality and its electrical behavior with a sub-pixel resolution is difficult to measure on this device.

#180110 - $15.00 USD Received 19 Nov 2012; revised 13 Jan 2013; accepted 14 Jan 2013; published 23 Jan 2013

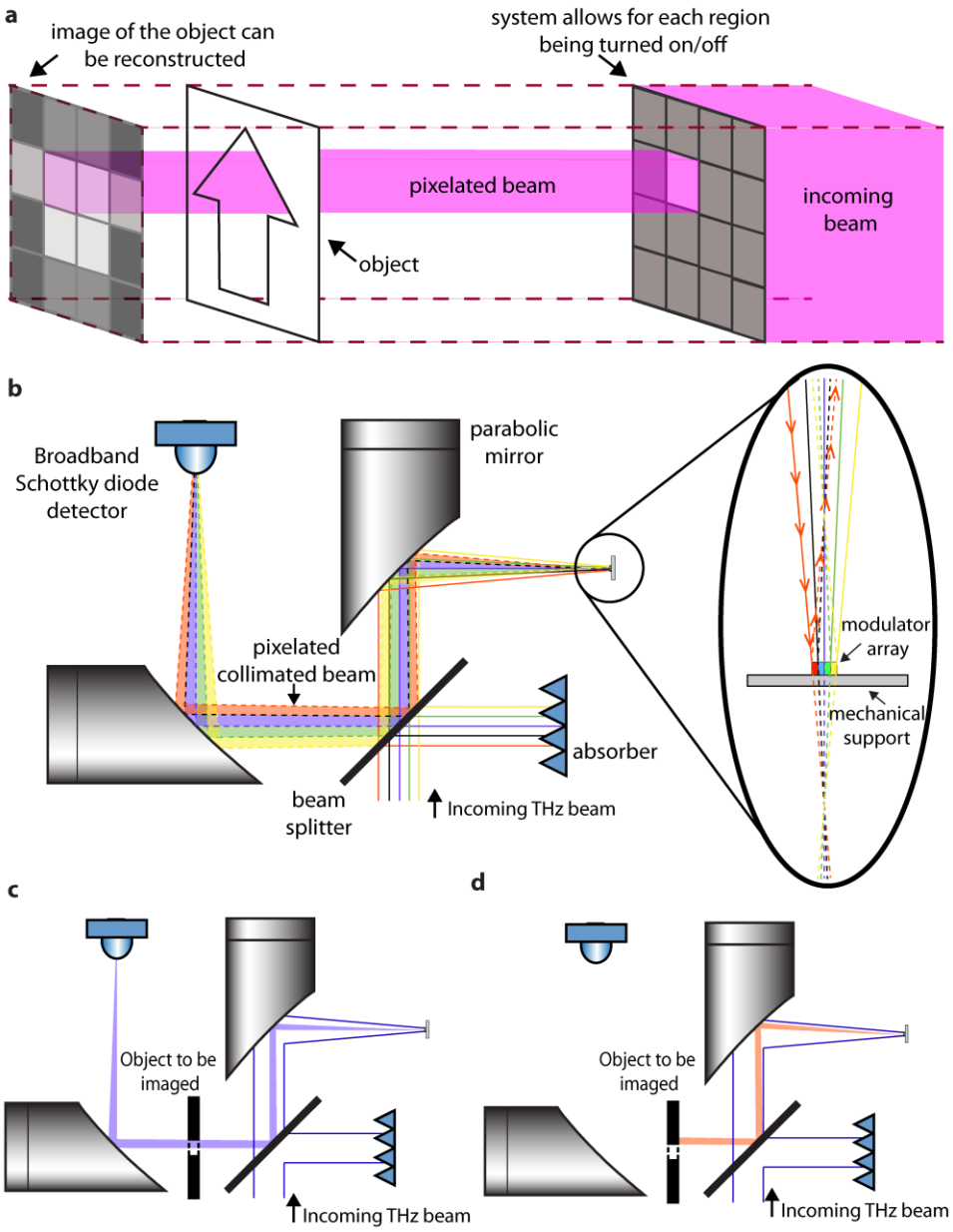

Fig. 3. Principle of the imaging experiment. (a) Sketch of an object in a pixelated and collimated illumination that is transformed by the modulator array. Each pixel of the illumination, denoted by different colors, can be turned on and off by the modulator array. (b) Sketch of the beam path showing the expanded beam is about the same size with the modulator array placed away from the focal plane so that the beam toward the detector is pixelated. No object is placed in the path of the beam. (c-d) Two pixels of illumination when an object is placed in the path of the beam.

4. Imaging experiments

The preliminary imaging experiments were carried out by placing the modulator array away from the focal plane, and we note that this imaging mechanism is different from the coded aperture approach [14]. In a highly simplified fashion, the imaging mechanism described in

#180110 - $15.00 USD Received 19 Nov 2012; revised 13 Jan 2013; accepted 14 Jan 2013; published 23 Jan 2013

this work can be viewed in Fig. 3(a). Together with mirrors, see Fig. 2(a) and Fig. 3(b), the modulator array with NxM pixels essentially transforms a point THz source into a pixelated and collimated beam of illumination as shown in Fig. 3(b). While keeping all other pixels off, i.e. no THz illumination from these pixels, we can switch on and off one pixel illumination thus transmittance of the corresponding part of the object under imaging can be detected. After sequentially operating all NxM pixels, the image of the object can be constructed.

To realize this mode of imaging, we place the modulator array away from the focal place so that the expanded beam is approximately the same size with the modulator array, as shown in Fig. 3(b). Since the focal length (~20 cm) is much larger than both the size of the modulator array (~3.5 mm x 3.5 mm) and the minimum beam waist (< ~1mm), normal incidence of the beam can still be assumed. Different colors sketched in the THz beam denote conceptually the pixelated illumination. To further illustrate the imaging procedure, let us turn to Fig. 3(c-d). The object is placed in the illuminated beam prior to the detector. While keeping all other pixels off (minimum reflectance), we switch on and off the i^{th} pixel (i.e. purple in Fig. 3(c) or red in Fig. 3(d)) and record the detector reading for this pixel: $\Delta R_i = R_{on,i} - R_{off,i}$. The spatial image of the object can be constructed by computing $\Delta R_i/\Delta R_{i0}$, where ΔR_i is the detector reading difference when the object is in place and ΔR_{i0} is that when there is no object. The switching speed of each pixel, given by the 3-dB cut-off of the modulation amplitude (see Ref [17].), was found to be near 6 kHz. It is important to recall that the highly resistive Si substrate has an adverse effect on the switching speed since it affects the effective capacitance and resistance of the device, both of which are voltage dependent, thus its RC time constant; however employing a highly resistive substrate allows for a reduction in the IL of the device due to a smaller free-carrier absorption by the substrate itself. Nonetheless, the measured switching speed suggests video rate imaging is possible, i.e. a 16x16 pixel array might image at 24 frames per second, a clear advantage over mechanical scanning.

Shown in Fig. 4(a) is a map of $\Delta R_{i0}/R_{0,low}$, where $R_{0,low}$ is the measured total reflectance when all the pixels are off (low reflectance) and ΔR_{i0} is the detector reading difference when switching on and off the i^{th} pixel without an object. As mentioned above, there are two pixels for which we didn't observe modulation, which are marked with a cross in Fig. 4. The non-uniformity of $\Delta R_{i0}/R_{0,low}$ is attributed to non-uniformity of the graphene quality [17, 18], and that in the power distribution of the THz beam over different pixels. Further optimization of the graphene quality and the optical setup, e.g. placing the modulator array in a collimated beam, or inserting an extra parabolic mirror prior to the array, demands future investigations. Nevertheless, the prototype setup shown in Fig. 3 allows for demonstrating the basic imaging function. Several examples (maps of $\Delta R_i/\Delta R_{i0}$) are shown in Fig. 4(b-d) using objects constructed using THz absorber material thus with little scattering. Sketches of these objects are shown below each map. It is observed that these maps closely resemble the shape of the objects. The system spatial resolution is determined by the pixel dimension of the pixelated collimated beam, which was estimated to be ~1.1cm. The dynamic range of the system, defined as the minimum of the ΔR_i versus noise floor ratio was found to be ~26 dB. In this imaging technique there is a tradeoff between the dynamic range and spatial resolution, since the smaller the collimated beam pixel, the smaller the ΔR_i thus dynamic range. Nevertheless, this prototype demonstration represents the first step toward developing THz imaging technologies utilizing graphene-based modulator arrays and, in the future, advanced algorithms such as coded aperture, which promise better system performance. Moreover, we also expect that other promising graphene-based modulator platforms such as active metamaterials [19, 25] and plasmonic devices [26, 27] be employed for imaging applications.

#180110 - $15.00 USD Received 19 Nov 2012; revised 13 Jan 2013; accepted 14 Jan 2013; published 23 Jan 2013

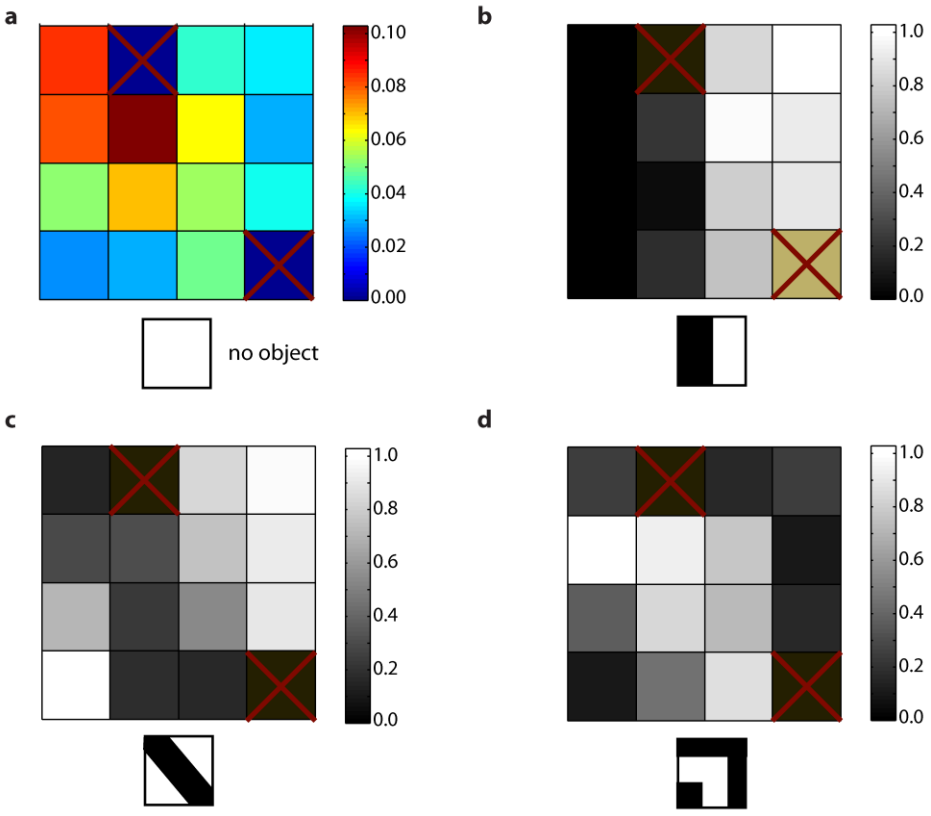

Fig. 4. (a) Map of "pixelated illumination" without an object: $\Delta R_{i0}/R_{0,low}$, where $R_{0,low}$ is the measured total reflectance when all the pixels are off, i.e. the minimum reflectance of the modulator array. (b-d) Map of $\Delta R_i/\Delta R_{i0}$ for three different objects placed in the path of the reflected beam. ΔR_i is the detected difference when switching the i^{th} pixel on and off while keeping all other pixels off. The two red crossed pixels crossed did not show modulation due to fabrication issues. The sketches of the objects made from the absorber material are shown below each map. The close resemblance between the map and the object indicates the graphene modulator array can be used for imaging.

5. Conclusion

We have presented a proof-of-concept experiment showing that arrays of graphene electro-absorption modulators can be employed for THz imaging applications. Since no mechanical parts are involved these devices can potentially enable low-cost video rate imaging systems.

Acknowledgments

The authors acknowledge the support from NSF (CAREER ECCS-084910, ECCS-1202452), AFOSR (FA9550-12-1-0257), the Center for Advanced Diagnostics and Therapeutics (AD&T) and the Center for Nanoscience and Technology (NDnano) at the University of Notre Dame.

#180110 - $15.00 USD Received 19 Nov 2012; revised 13 Jan 2013; accepted 14 Jan 2013; published 23 Jan 2013